

Flowing Gauge Theories: Finite-Density QED_{1+1}

Henry Lamm*

University of Maryland

E-mail: hlamm@umd.edu

Finite-density calculations in lattice field theory are typically plagued by sign problems. A promising way to ameliorate this issue is the *holomorphic flow* equations that deform the manifold of integration for the path integral to manifolds in the complex space where the sign fluctuations are less dramatic. We discuss some novel features of applying the flow equations to gauge theories and present results for finite-density QED_{1+1} .

The 36th Annual International Symposium on Lattice Field Theory - LATTICE2018
22-28 July, 2018
Michigan State University, East Lansing, Michigan, USA.

*Speaker.

Observables in non-perturbative field theory are typically calculated via stochastic methods and importance sampling. Alas, at finite density the action is complex, resulting in a non-real Boltzmann factor e^{-S} that rapidly oscillates as a function of field variables. This presents a challenge due to strong cancellations between regions. This *sign problem* is the main roadblock to the lattice QCD study of dense matter.

If instead of evaluating the path integral over real fields, but as an integral over a chosen integration contour in complex field space, the sign problem can be ameliorated. Cauchy's theorem guarantees that, for classes of contours, the value of the path integral is unchanged. The original suggestion [1, 2, 3, 4] was to use a certain combination, \mathcal{M}_T , of *Lefschetz thimbles*. To avoid the difficulties of this method, in [5], a so-called *generalized thimble method* (GTM) was proposed, in which a manifold \mathcal{M}_T is obtained by continuously deforming \mathbb{R}^N via the *holomorphic flow equation*: $\frac{d\phi_i}{dt} = \frac{\partial S}{\partial \phi_i}$. Evolving every point of \mathbb{R}^N for a "time" T , \mathcal{M}_T is obtained that i) yields equivalent results to the original space and ii) approaches \mathcal{M}_T in the limit $T \rightarrow \infty$, improving the sign problem. Other manifolds have also been used to reduce computational costs [6, 7, 8, 9, 10, 11].

Apply these methods to gauge theories has developed slowly with only 0+1 dimensional models, one-plaquette models [12] and QED₁₊₁ [13] being studied. Gauge invariance brings a host of conceptual issues, which must be understood in the context of GTM. Unlike previously-studied models, the thimble decomposition in QED₁₊₁ is not well-defined; despite this GTM yields correct results and improves the sign problem.

The thermal expectation value of an observable \mathcal{O} are given by

$$\langle \mathcal{O} \rangle = \frac{\int_{\mathbb{R}^N} \mathcal{D}\phi \mathcal{O} e^{-S}}{\int_{\mathbb{R}^N} \mathcal{D}\phi e^{-S}} = \frac{\int_{\mathcal{M}} \mathcal{D}\phi \mathcal{O}[\phi] e^{-S[\phi]}}{\int_{\mathcal{M}} \mathcal{D}\phi e^{-S[\phi]}}. \quad (1)$$

where \mathcal{M} is a manifold in complex field space. The average sign is

$$\langle \sigma \rangle \equiv \left\langle e^{-iS_I} \right\rangle_{S_R} = \frac{\int \mathcal{D}\phi e^{-S}}{\int \mathcal{D}\phi e^{-S_R}}. \quad (2)$$

Inspecting this expression leads to a conceptual understanding of how the sign problem is reduced. The numerator has a holomorphic integrand, thus independent of \mathcal{M} . However, the denominator's integrand is *not* holomorphic and $\langle \sigma \rangle$ thus depends on \mathcal{M} . We parametrize every point $\tilde{\phi}_T(\phi)$ on \mathcal{M}_T by the real coordinates in ϕ . Using ϕ , the expectation values can be written as

$$\langle \mathcal{O} \rangle = \frac{\int_{\mathcal{M}_T} \mathcal{D}\tilde{\phi} \mathcal{O}[\tilde{\phi}] e^{-S[\tilde{\phi}]}}{\int_{\mathcal{M}_T} \mathcal{D}\tilde{\phi} e^{-S[\tilde{\phi}]}} = \frac{\int_{\mathbb{R}^N} \mathcal{D}\phi \mathcal{O}[\tilde{\phi}_T(\phi)] e^{-S[\tilde{\phi}_T(\phi)]} \det J}{\int_{\mathbb{R}^N} \mathcal{D}\phi e^{-S[\tilde{\phi}_T(\phi)]} \det J} \quad (3)$$

where we introduce the Jacobian matrix given by $J_{ij} = \frac{\partial(\tilde{\phi}_T)_i}{\partial \phi_j}$.

In the limit $T \rightarrow \infty$, most fields acquire large S_R and decouple from the path integral. In the real-field parameterization, the path integral's support comes from the points that flow into small regions near the critical points. These regions are stretched by flow and generate N -real-dimensional surfaces around the critical points. In other words, in the large T limit, \mathcal{M}_T is the union of approximate thimbles attached to these critical points.

Since S_I is constant with flow, so the variation of S_I on an approximate thimble is small. Consequently the sampled fields has a small phase variation, hence a milder sign problem¹.

As a demonstration of the generalized thimble method in a gauge theory, we study a three-flavor QED in 1+1 dimensions. The action is

$$S = \frac{1}{g^2} \sum_r (1 - \cos P_r) - \sum_a \ln \det D^{(a)} \quad (4)$$

where $D^{(a)}$ denotes the fermionic matrix for flavor a , and P_r denotes the primitive plaquette with r at the lower-right corner $P_r \equiv A_1(r) + A_0(r + \hat{x}) - A_1(r + \hat{t}) - A_0(r)$. Above \hat{t} and \hat{x} are the unit vectors in time and space direction. We discretize the fermion action using the staggered formulation. The Kogut-Susskind staggered fermion matrix for flavor a is given by

$$D_{xy}^{(a)} = m_a \delta_{xy} + \frac{1}{2} \sum_{\nu \in \{0,1\}} [\eta_\nu e^{iQ_a A_\nu(x) + \mu \delta_{\nu 0}} \delta_{x+\hat{\nu}, y} - \eta_\nu e^{-iQ_a A_\nu(x) - \mu \delta_{\nu 0}} \delta_{x, y+\hat{\nu}}]. \quad (5)$$

All flavors have the same mass $m_a = m$ and chemical potential μ_Q but with charge assignments $Q_1 = Q_+ = +2$, and $Q_{2,3} = Q_- = -1$.

Previous arguments that GTM improves the sign problem relied upon \mathcal{M}_T approaching the Lefschetz thimbles at $T \rightarrow \infty$. Where no such unique thimble decomposition exists, it is not obvious what the large- T limit of \mathcal{M}_T is, and whether the sign problem is reduced.

In QED₁₊₁ dimensions, there are two separate obstacles to defining a unique thimble decomposition: critical points are degenerate (the action does not change along gauge orbits), and lines of flow may connect one critical point to another (Stokes' phenomenon).

A Lefschetz thimble is defined from an isolated critical point z_c as the union of all solutions $\lim_{T \rightarrow -\infty} z(T) = z_c$. For a holomorphic function of N complex variables, each isolated critical point is a saddle point with N stable and N unstable directions; therefore, each Lefschetz thimble is an N -real-dimensional surface. However, in a gauge theory, all critical points form gauge orbits and therefore unisolated.

For an abelian theory like QED₁₊₁, the gauge degeneracies can be resolved by gauge-fixing. In the complexified field space a general gauge transformation is given by

$$A_\mu(x) \rightarrow A_\mu(x) + \alpha(x + \hat{\mu}) - \alpha(x) \quad (6)$$

where $\alpha(x)$ is any complex-valued function on the lattice points and $\hat{\mu}$ denotes the unit vector along the direction $\mu \in \{0,1\}$. With V lattice sites, the complexified field space is \mathbb{C}^{2V} . The gauge orbit of any configuration $A_{x,\mu}$ is obtained by adding to it all vectors of the form $\alpha(x + \mu) - \alpha(x)$, for every $\alpha(x)$ implying a $(V - 1)$ -dimensional space since $\alpha(x) = \alpha$ is trivial. Every $A_\mu(x)$ can be decomposed $A_\mu(x) = A_\mu^\perp(x) + A_\mu^\parallel(x)$, with $A_\mu^\parallel(x)$ parallel to the gauge orbit and $A_\mu^\perp(x)$ orthogonal to it. We can choose $A_\mu^\perp(x)$ as the representative of $A_\mu(x)$ in every gauge orbit. In this way, we decompose the original real configuration space as $\mathbb{R}^{2V} = \mathcal{M}_0 \oplus \mathcal{G}$, where $\mathcal{M}_0 = \mathbb{R}^{V+1}$ is the gauge-fixed space of $A_\mu^\perp(x)$, and \mathcal{G} is a single gauge orbit. The gradient $\frac{\partial S}{\partial A}$ is orthogonal to the gauge orbits so a gauge-fixed

¹Provided the residual phase from $\text{Im} \det J$ and cancellations *between* thimbles are negligible.

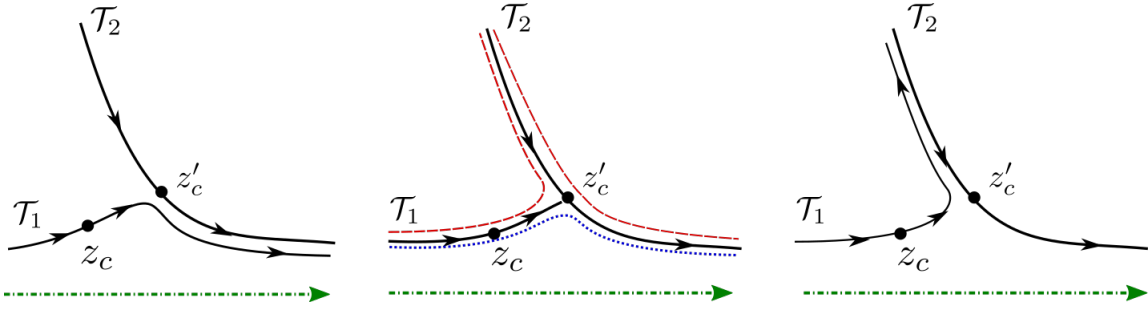


Figure 1: A schematic view of Stokes' phenomenon. The original integration contour is given by the dash-dotted green line. The solid dots denote the critical points, solid lines denote different thimbles, and the arrows denote the orientation of the thimbles. As the argument of S changes (from left to right), the thimble decomposition jumps from \mathcal{T}_1 (left) to $\mathcal{T}_1 + \mathcal{T}_2$ (right). When Stokes' phenomenon occurs (center) there is no unique thimble decomposition, which we indicate by two paths of integration given by the red dashed and blue dotted lines.

slice, defined by constant $A_\mu^\parallel(x)$, is invariant under the flow. Critical points are isolated in each slice, and a unique definition of the thimble decomposition exists. The behavior of flow can be understood by considering each slice. Since gauge fixing and flow commute, flowing the entire gauge-free integration domain is $\mathcal{M}_T \oplus \mathcal{G}$. In simulations, no gauge fixing is performed, so they perform a random walk in \mathcal{G} .

The second difficulty encountered in the decomposition is Stokes' phenomenon, where a flow line connects two critical points. The left and right panels of Fig. 1 show the flow assuming adding a small $i\epsilon$ to the action with opposite signs. In each case, the thimble decomposition is well-defined, but \mathcal{M}_T equivalent to the real domain is different. Stokes' phenomenon affects the behavior of the holomorphic flow. In the case of QED_{1+1} , it occurs at all μ and g . While Stokes' phenomenon does not cause any discontinuity in the flowed manifolds, it does produce undesirable "bumps". As T increases, a bump is created near the origin. The effect can be understood by considering the $T \rightarrow \infty$ limit, where it is maximized. In this limit, the bump travels up one half of the imaginary axis, and directly back down again, producing a closed contour of integration. The sum of these two segments cancel but the average sign is decreased by their presence.

To separate the effect of the phase fluctuations on \mathcal{M}_T and the fluctuations induced by approximating $\ln \det J$ with W , we write the reweighting factor $\Delta S = i \text{Im} S_{\text{eff}} + \Delta J$. The phase factor $\exp(-i \text{Im} S_{\text{eff}})$ is a pure phase. The real factor ΔJ , with $\exp(-\Delta J) = |\det J|/|W|$, is necessary to correct for using W instead of $\det J$ in the Monte-Carlo process.

The speed-up from GTM compared to real-plane calculations is given in terms of: t_{config} , the wall-clock time required to generate a configuration; $\langle \sigma \rangle$, the average sign; and Σ , the *statistical power* defined via $w = e^{-\Delta J} / \langle e^{-\Delta J} \rangle_{S'_{\text{eff}}}$. The expression for Σ is

$$\Sigma \equiv \frac{\langle w \rangle_{S'_{\text{eff}}}}{\langle w^2 \rangle_{S'_{\text{eff}}}} = \frac{1}{\langle w^2 \rangle_{S'_{\text{eff}}}}. \quad (7)$$

Σ is bounded between $1/n_{\text{config}}$ and 1 and is an estimate of the fraction of configurations that effectively contribute. A small value of Σ indicates that the averages are dominated by

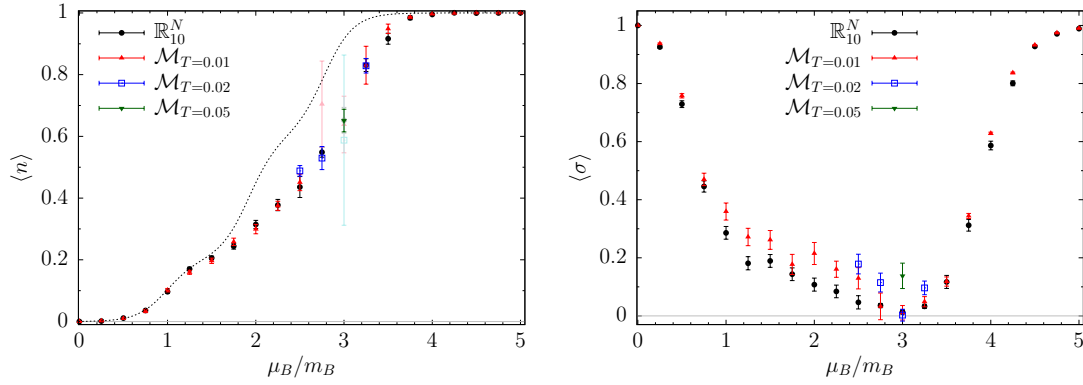


Figure 2: Density $\langle n \rangle$ and average sign $\langle \sigma \rangle$ as a function of μ_B/m_B for staggered fermions on a lattice of size 10×10 . The dashed curve represents the free baryon gas with the same mass.

a small number of configurations and, consequently, more configurations need to be used for a reliable estimate.

A figure of merit h_T for a fixed flow time T can be defined as $h_T = \frac{\langle \sigma \rangle^2 \Sigma}{t_{\text{config}}}$. A ratio h_{T_1}/h_{T_2} estimates the relative speed-up of flow time T_1 over flow time T_2 . $\langle \sigma \rangle$ should increase with T because flowing improves the relative sign, but t_{config} also increases because longer flow requires more computational time. Due to the use of W , an approximate Jacobian that is computationally faster, the statistical reweighting plays a nontrivial part.

The bare parameters $g = 0.5$ and $m = 0.05$ yield the renormalized baryon mass $am_B \approx 0.6$, below the lattice cutoff scale. We have undertaken calculations on a fixed spatial lattice size $n_x = 10$ at three different inverse temperatures $n_t = 6, 10, 14$. The fermion density and $\langle \sigma \rangle$ are presented for a 10×10 lattice in Fig. 2. Consistent results for the density are found, while $\langle \sigma \rangle$ increases with larger T . On the colder lattice, 14×10 , one sees the *Silver Blaze* phenomenon at small μ_B/m_B in Fig. 3, as well as development of a plateau at the one baryon threshold. Sample h_T/h_0 for the $n_t = 10$ lattice are in Table 1. h_T for some μ_B/m_B exceeds unity on both lattices, implying flow reduces the computational time.

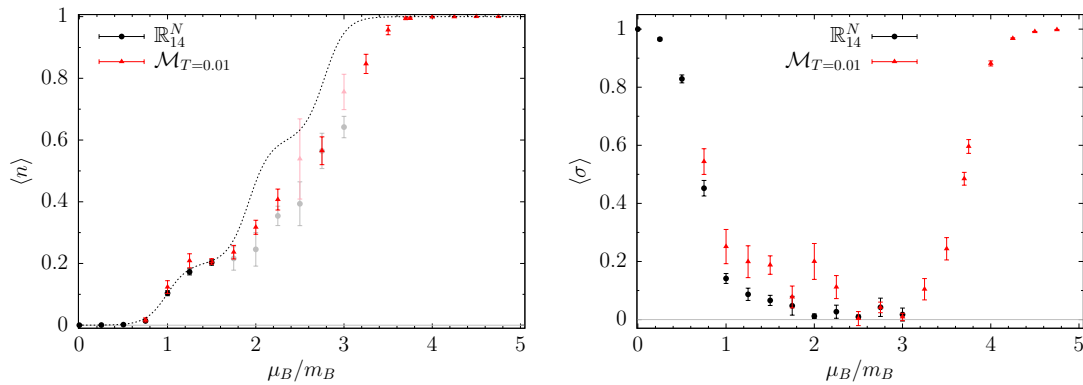


Figure 3: Density $\langle n \rangle$ and average sign $\langle \sigma \rangle$ as a function of μ_B/m_B for staggered fermions on a lattice of size 14×10 . The dashed curve represents the free baryon gas with the same mass.

GTM may be applied to gauge theories without encountering any fundamental obstacles,

T	$t_{\text{config},T}/t_{\text{config},0}$	Σ_T/Σ_0	$\langle\sigma\rangle_T/\langle\sigma\rangle_0$	h_T/h_0
0.01	6	0.8	3	1.2
0.02	18	0.7	4	0.6
0.05	28	0.5	13	3

Table 1: Maximum figure of merit h_T/h_0 for different flow times T measured on the 10×10 lattice.

as shown in QED₁₊₁. The difficulties that plague the definition of Lefschetz thimbles in a gauge theory are found to be innocuous. Despite the holomorphic flow requiring greater computational time per configuration compared to the real plane, the improvement in the average sign reduces the time needed to compute observables at a fixed precision compared to an equivalent real plane calculation.

Acknowledgments

The work was completed in collaboration with Andrei Alexandru, Gocke Basar, Paulo Bedaque, and Scott Lawrence, all of whom the author would like to thank. H.L. is supported by U.S. Department of Energy under Contract No. DE-FG02-93ER-40762.

References

- [1] AURORASCIENCE, M. Cristoforetti, F. Di Renzo and L. Scorzato, *New approach to the sign problem in quantum field theories: High density QCD on a Lefschetz thimble*, *Phys. Rev.* **D86** (2012) 074506 [[1205.3996](#)].
- [2] M. Cristoforetti, F. Di Renzo, A. Mukherjee and L. Scorzato, *Monte Carlo simulations on the Lefschetz thimble: Taming the sign problem*, *Phys. Rev.* **D88** (2013) 051501 [[1303.7204](#)].
- [3] M. Cristoforetti, F. Di Renzo, A. Mukherjee and L. Scorzato, *Quantum field theories on the Lefschetz thimble*, *PoS LATTICE2013* (2014) 197 [[1312.1052](#)].
- [4] L. Scorzato, *The Lefschetz thimble and the sign problem*, *PoS LATTICE2015* (2016) 016 [[1512.08039](#)].
- [5] A. Alexandru, G. Basar, P. F. Bedaque, G. W. Ridgway and N. C. Warrington, *Sign problem and Monte Carlo calculations beyond Lefschetz thimbles*, *JHEP* **05** (2016) 053 [[1512.08764](#)].
- [6] A. Alexandru, P. F. Bedaque, H. Lamm and S. Lawrence, *Deep Learning Beyond Lefschetz Thimbles*, *Phys. Rev.* **D96** (2017) 094505 [[1709.01971](#)].
- [7] Y. Mori, K. Kashiwa and A. Ohnishi, *Toward solving the sign problem with path optimization method*, *Phys. Rev.* **D96** (2017) 111501 [[1705.05605](#)].
- [8] A. Alexandru, P. F. Bedaque, H. Lamm and S. Lawrence, *Finite-Density Monte Carlo Calculations on Sign-Optimized Manifolds*, [1804.00697](#).
- [9] Y. Mori, K. Kashiwa and A. Ohnishi, *Application of a neural network to the sign problem via the path optimization method*, *PTEP* **2018** (2018) 023B04 [[1709.03208](#)].
- [10] F. Bursa and M. Kroyter, *A simple approach towards the sign problem using path optimisation*, [1805.04941](#).

- [11] A. Alexandru, P. F. Bedaque, H. Lamm, S. Lawrence and N. C. Warrington, *Fermions at Finite Density in $(2+1)d$ with Sign-Optimized Manifolds*, [1808.09799](#).
- [12] C. Schmidt and F. Ziesche, *Simulating low dimensional QCD with Lefschetz thimbles*, *PoS LATTICE2016* (2017) 076 [[1701.08959](#)].
- [13] A. Alexandru, G. Basar, P. F. Bedaque, H. Lamm and S. Lawrence, *Finite Density QED_{1+1} Near Lefschetz Thimbles*, *Phys. Rev.* **D98** (2018) 034506 [[1807.02027](#)].